A coupled fluorescence assay for high-throughput screening of polyurethane-degrading enzymes

Liujun YANG[a], Xianjun DENG[a], Renju LIU[b], Jianyang LI[b], Junyao ZHAI[a], Xiaoxiao MA[a], Shiyang YOU[a], Qinghao HE[c], Arthur K.L. LIN[c], Zongze SHAO[b], Jiguang WANG[d],Hongyuan LU[a]*

[a] *Thrust of Bioscience and Biomedical Engineering, The Hong Kong University of Science and Technology (Guangzhou), Guangzhou 511400, China*

[b] *Key Laboratory of Marine Genetic Resources, Third Institute of Oceanography, Ministry of Natural Resources, Xiamen 361005, China*

[c] *College of Future Technology, The Hong Kong University of Science and Technology (Guangzhou), Guangzhou 511400, China*

d Division of Life Science, Department of Chemical and Biological Engineering, The Hong Kong University of Science and Technology, Clear Water Bay, Kowloon, Hong Kong SAR, China

Corresponding authors: Hongyuan LU (hongylu@hkust-gz.edu.cn)
First author contact: Liujun YANG (lyang068@connect.hkust-gz.edu.cn)

Abstract

The global accumulation of plastic waste, including polyurethane (PU), demands urgent solutions. Enzymatic depolymerization offers a viable strategy for PU waste valorization. However, the lack of reliable high-throughput screening (HTS) assays for PU-degrading enzymes has hindered progress. Conventional methods are limited by either poor substrate relevance or inadequate quantification, limiting their industrial applicability and predictive accuracy. Here, we developed a HTS assay integrating a chemically defined, synthetic poly(ethylene adipate)-based PU (PEA-PU) substrate with a sensitive fluorescence-based detection cascade. Upon enzymatic hydrolysis, PEA-PU releases stoichiometric amounts of adipic acid and ethylene glycol, the latter converted to resorufin via a two-enzyme system (glycerol dehydrogenase and diaphorase). This assay enables rapid quantification, molecular-level monitoring of PU degradation with high reproducibility and sensitivity. Validation using known PU-degrading enzymes (ICCM and BaCut1) demonstrated strong correlation between fluorescence-derived ethylene glycol levels and chromatographic measurements, confirming quantitative accuracy. Unlike commercial substrates, our assay establishes clear structure-activity relationships while enabling direct product quantification. Demonstrating the assay's utility, we screened a focused library of BaCut1 variants and rapidly identified mutants with superior efficacy against both synthetic substrates and commercial PU foam. Ultimately, this work bridges the gap between high-throughput capacity and material relevance, providing a scalable pipeline to accelerate the discovery and engineering of enzymes for real-world PU plastic valorization.

Environmental Implication

Polyurethane (PU) pollution threatens ecosystems worldwide, as conventional disposal methods like landfilling and incineration cause lasting harm. To address this, we developed a high-throughput fluorescence assay using a chemically defined PU substrate to quantitatively evaluate enzymatic degradation. This standardized method accelerates the discovery of novel PU-degrading enzymes from microbial communities and aids in engineering improved biocatalysts. By enabling efficient identification and optimization of these enzymes, our work advances biological solutions for persistent plastic waste. The assay supports enzymatic recycling processes that could reduce reliance on landfilling and incineration, promoting cleaner ecosystems and a circular plastics

economy. This approach offers a practical tool for sustainable PU waste management.

Graphical Abstract

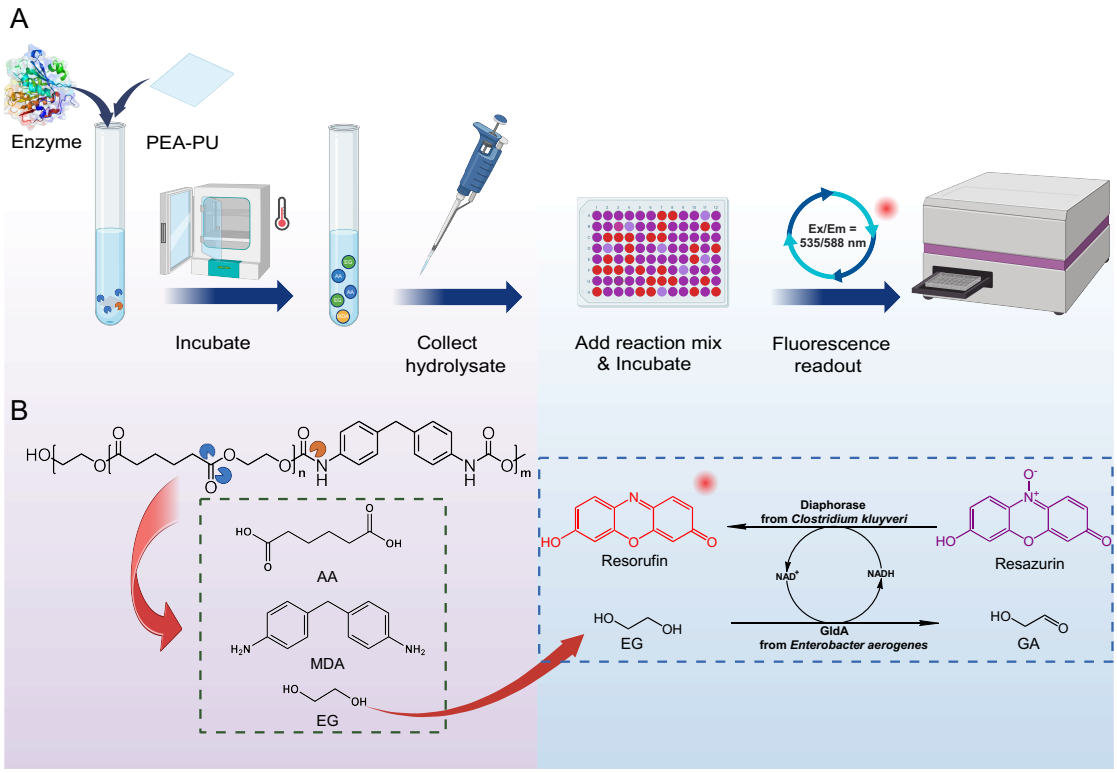

(A) Schematic overview of the coupled fluorescence assay workflow for high-throughput screening (HTS) of polyurethane (PU)-degrading enzymes. Enzymes are incubated with chemically defined poly(ethylene adipate)-based PU (PEA-PU) films. The resulting hydrolysate, which primarily contains ethylene glycol (EG, detectable via the assay) and adipic acid (AA) as characteristic degradation products, is collected and analysed using a fluorescence-based assay in microplate format (Ex/Em = 535/588 nm). **(B) Working principle of the coupled fluorescence assay**. The assay detects EG through a two-step enzymatic cascade: (1) Glycerol dehydrogenase (GldA) oxidizes EG to glyoxylic acid (GA) while reducing NAD^+ to NADH; (2) Diaphorase then utilizes NADH to convert resazurin into fluorescent resorufin (Ex/Em = 535/588 nm). This stoichiometric conversion enables quantitative monitoring of PU degradation activity.

"Keywords: polyurethane; biodegradation; high-throughput screening; enzyme engineering; fluorescence assay;"

1 Introduction

Plastic pollution poses a pressing global challenge, threatening ecosystems [1-3] and human health [4–9]. A major contributor to this crisis is polyurethane (PU), a synthetic polymer extensively used in foams (e.g., mattresses, insulation), elastomers (e.g., shoe soles, medical devices), and durable goods (e.g., automotive parts, synthetic leather) [10–12]. Given the low recycling rate of PU waste [12,13], its environmental persistence highlights the urgent need for sustainable solutions [13–16].

Enzymatic depolymerization has emerged as a promising strategy for PU waste valorization, attracting growing research interest [10,13–15,17,18]. However, progress in this field remains limited. This is largely due to persistent challenges in identifying, characterizing, and engineering enzymes that can efficiently degrade PU under industrial conditions [14–23].

A major bottleneck lies in current enzyme screening assays (Table 1), which suffer from limitations in predictive accuracy and practical utility. Conventional assays using low-molecular-weight model substrates (e.g., *p*-nitrophenyl esters or carbamates) often fail to predict enzyme activity against authentic polymeric PU, leading to false positives that misdirect enzyme discovery efforts [14,15,17,19]. In contrast, while industrial PU materials (e.g., foams, films, elastomers) offer greater physiological relevance, their heterogeneity and slow degradation kinetics render them unsuitable for high-throughput screening (HTS) applications [15,18,20,21]. Furthermore, while recent innovations in nanosensors [24] and microfluidics [25] have successfully increased throughput, these platforms often rely on indirect surrogate probes that fail to accurately reflect authentic solid PU degradation.

Consequently, many studies have turned to colloidal PU dispersions (e.g., Impranil DLN or Bayhydrol), accessing enzyme activity via clearing zone formation [26] or by monitoring OD reduction in PU emulsions upon enzyme or microbial addition [27]. However, these proprietary mixtures are chemically undefined and only detect bulk esterase activity. These limitations hinder rigorous quantitative analysis, which is crucial for enzyme discovery and mechanistic studies [14,15,20,24].

To overcome these limitations, we developed an HTS assay using a synthetic PU substrate designed to release detectable degradation products upon enzymatic hydrolysis. By coupling this reaction to a detection cascade that enzymatically converts degradation products into an optical signal, we enable real-time kinetic measurements and direct activity comparisons.

This assay resolves key ambiguities in existing methods by delivering a quantitative, high-throughput measurement of PU hydrolysis kinetics, enabling rapid and precise enzyme variants screening. Rigorous validation with established PU-degrading enzymes confirms its high sensitivity, reproducibility, and robustness. To demonstrate its practical utility, we applied this framework to screen a BaCut1 saturation-mutagenesis library, successfully identifying variants with enhanced activity against both poly (ethylene adipate) (PEA)-PU and commercial PU foam.

Feature	LMW Model Compounds	PU Dispersions	Commercial PU Materials
Representative Examples	*p*-Nitrophenyl esters, carbamates	Impranil® DLN, Bayhydrol® 110	PU foam, film, elastomer
Chemical Definition	Defined, synthetic molecules	Proprietary formulations	Undefined mixtures or composites
Physiological Relevance	Low	Moderate	High
Readout Modality	Colorimetric absorbance	Turbidity clearing, halo formation	Weight loss, SEM, product analysis (e.g., HPLC)
Data Quality	Quantitative (model-limited)	Non-quantitative	Quantitative (method-dependent)
Screening Throughput	High	Moderate	Low
Bond-Type Specificity	Restricted to designed motifs	Ester-biased; limited urethane sensitivity	Broad; structurally diffuse
Mechanistic Insight	Indirect; lacks polymer context	Partial; limited structural resolution	Direct, but labor-intensive

Table 1: Critical limitations of current assay formats for PU biodegradation. A comparative overview of model substrates, colloidal PU dispersions, and commercial PU materials used in PU degradation assays.

2 Results and Discussion

2.1 Synthesis and characterization of PEA-PU

To develop a quantitative assay for PU-degrading enzymes, we designed a novel polymeric substrate that is chemically well-defined and readily synthesizable. The polymer features a soft segment composed of PEA. Hydrolysis of its ester bonds produces two well-defined products: ethylene glycol (EG) and adipic acid (AA). Both can be easily quantified with high reliability. Specifically, the PEA-PU polymer was synthesized via a one-step, solvent-based step-growth polymerization [27,29] (Fig. 1A). The resulting polymer solution was then cast into films exhibiting high optical transparency and uniformity (Fig. 1B). This optical quality reflects excellent macroscopic homogeneity, which is desirable for consistent enzyme-substrate interactions in replicate assays.

To confirm the polymer's chemical composition, we performed ^{1}H NMR analysis. The ^{1}H NMR spectrum (Fig. 1C) exhibited three diagnostic regions that unambiguously confirmed the polyester–urethane backbone architecture: (i) the urethane N–H proton at δ 9.63 ppm; (ii) aromatic and bridging methylene protons from the MDI-based hard segment at δ 7.07–7.35 and 3.78 ppm, respectively; (iii) O-linked methylene protons from the ethylene glycol units at δ 4.18–4.29 ppm, and aliphatic methylene protons from the adipate segment at δ ~2.3 and ~1.5 ppm. These clearly assignable signals demonstrate successful formation of both urethane and ester linkages in the polymer structure, providing a structural foundation for precise analysis of enzymatic degradation.

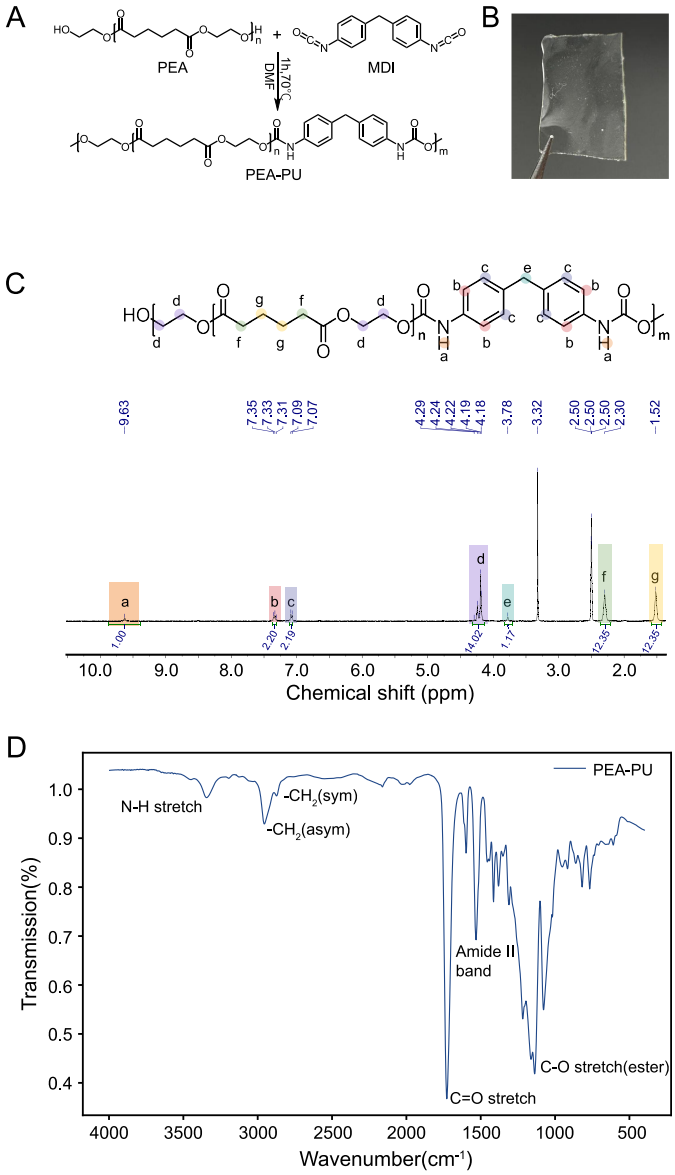

Figure 1: Synthesis and characterization of poly (ethylene adipate)-polyurethane (PEA-PU). (A) Synthesis of PEA-PU via step-growth polymerization. PEA-PU was synthesized by reacting pre-dried polyethylene adipate (PEA, Mn ≈ 1000 g/mol) with 4,4′-methylenebis (phenyl isocyanate) (MDI) at an NCO: OH molar ratio of 1:1 in anhydrous DMF at 70 °C under a nitrogen atmosphere for 1 hour. **(B) PEA-PU film**. The polymer solution was cast into a PTFE mold and dried under vacuum at 60 °C for 24 hours, yielding a film approximately 0.2 mm thick. **(C) ¹H-NMR spectrum of PEA-PU**. δ 9.63 (br s, NH, urethane); 7.33 (t, J ≈ 8.6 Hz, 2 H) & 7.08 (d, J ≈ 8.2 Hz, 3 H) = aromatic H of MDI; 4.40–4.15 (m, ≈14 H) = overlapped O-CH_2-CH_2-O and α-CH_2 next to carbonyl/urethane O; 3.78 (br s, Ar-CH_2-Ar bridge, down-field half; up-field partner at ~3.3 ppm is buried in the 2.6–2.3 ppm envelope); 2.60–2.35 (br m) = overlapped Ar-CH_2-Ar partner + urethane α-CH_2 ± minor end groups; 2.30 (br s) = adipate α-CH_2; 1.52 (br s) = internal aliphatic CH_2. **(D) FTIR spectrum of PEA-PU.**The spectrum exhibits characteristic absorption bands, including a composite carbonyl band at 1725 cm^{-1} (overlapping ester and urethane C=O stretches), a urethane N–H stretch at 3320 cm^{-1}, an amide II band at 1530 cm^{-1} (N–H bending coupled with C–N stretching), and an amide III/ester C–O–C band at 1240 cm^{-1}, collectively validating the expected urethane and ester functionalities in the polymer backbone.

Complementary structural verification was achieved through Fourier-transform infrared (FTIR) spectroscopy (Fig. 1D; Fig. S1). The spectrum displayed all expected characteristic absorptions: (i) a strong ester C=O stretch at 1725 cm^{-1}, (ii) a broad urethane N–H stretch at 3320 cm^{-1}, (iii) an amide II band (C–N stretch) at 1530 cm^{-1}, and (iv) an ester C–O stretch at 1240 cm^{-1}. These features showed excellent agreement with reference spectra of urethane and ester groups, supporting the expected chemical structure of the polymer.

To further validate the material's properties, we characterized the thermal behavior of the synthesized PEA-PU using differential scanning calorimetry (DSC). The DSC results revealed that PEA-PU exhibits amorphous thermoplastic behavior, with a glass transition temperature of approximately –17.6 °C, as determined by the half-height method (Fig. S2). No melting transition was observed up to 200 °C. This thermal profile confirms the absence of crystalline domains, making the material particularly suitable for enzymatic degradation studies [15,23,30,31].

Taken together, these results demonstrate that PEA-PU is a structurally uniform, chemically well-defined polymer with straightforward synthesis and characterization. The material is optically transparent and exhibits distinct spectroscopic signatures, facilitating analytical tracking. More importantly, PEA-PU closely replicates the structural and chemical properties of post-consumer PU waste, making it a highly representative model system. These properties establish PEA-PU as an ideal model substrate for enzymatic degradation studies while also serving as a reproducible, standardized platform for developing robust PU degradation assays.

2.2 Enzymatic degradation of PEA-PU

Following comprehensive characterization of PEA-PU's structure and physicochemical properties, we next evaluated its enzymatic degradability using two well-characterized polyester hydrolases: ICCM (an engineered leaf compost cutinase variant) and BaCut1 (a cutinase from *Blastobotrys* sp. G-9) [32,33]. Although both enzymes demonstrate PU-degrading capability, prior studies have reported that ICCM exhibit greater polyester hydrolytic activity than BaCut1 under their respective optimal conditions [32,33]. We therefore employed PEA-PU as a model substrate to determine whether this documented activity difference could be reliably replicated, assessing its potential for standardized enzyme performance comparisons.

PEA-PU films were incubated with each enzyme for 36 hours under their optimal conditions (70 °C for ICCM, 37 °C for BaCut1). Enzymatic treatment induced significant morphological alterations in the films, which transitioned from an initially transparent state to an opaque and fragmented morphology (Fig. 2A). In contrast, control samples exhibited no structural or optical changes, demonstrating that the degradation was exclusively enzyme dependent.

To examine surface-level enzymatic degradation, we analyzed PEA-PU films by scanning electron microscopy (SEM). While untreated films displayed smooth and uniform surfaces, enzyme-treated samples exhibited significant surface erosion (Fig. 2A). ICCM treatment induced pronounced degradation features, including deep pits and porous structures, whereas BaCut1 treatment caused milder surface disruption. These distinct morphological patterns reflect differential catalytic efficiencies between the two enzymes, consistent with previous reports [32,33].

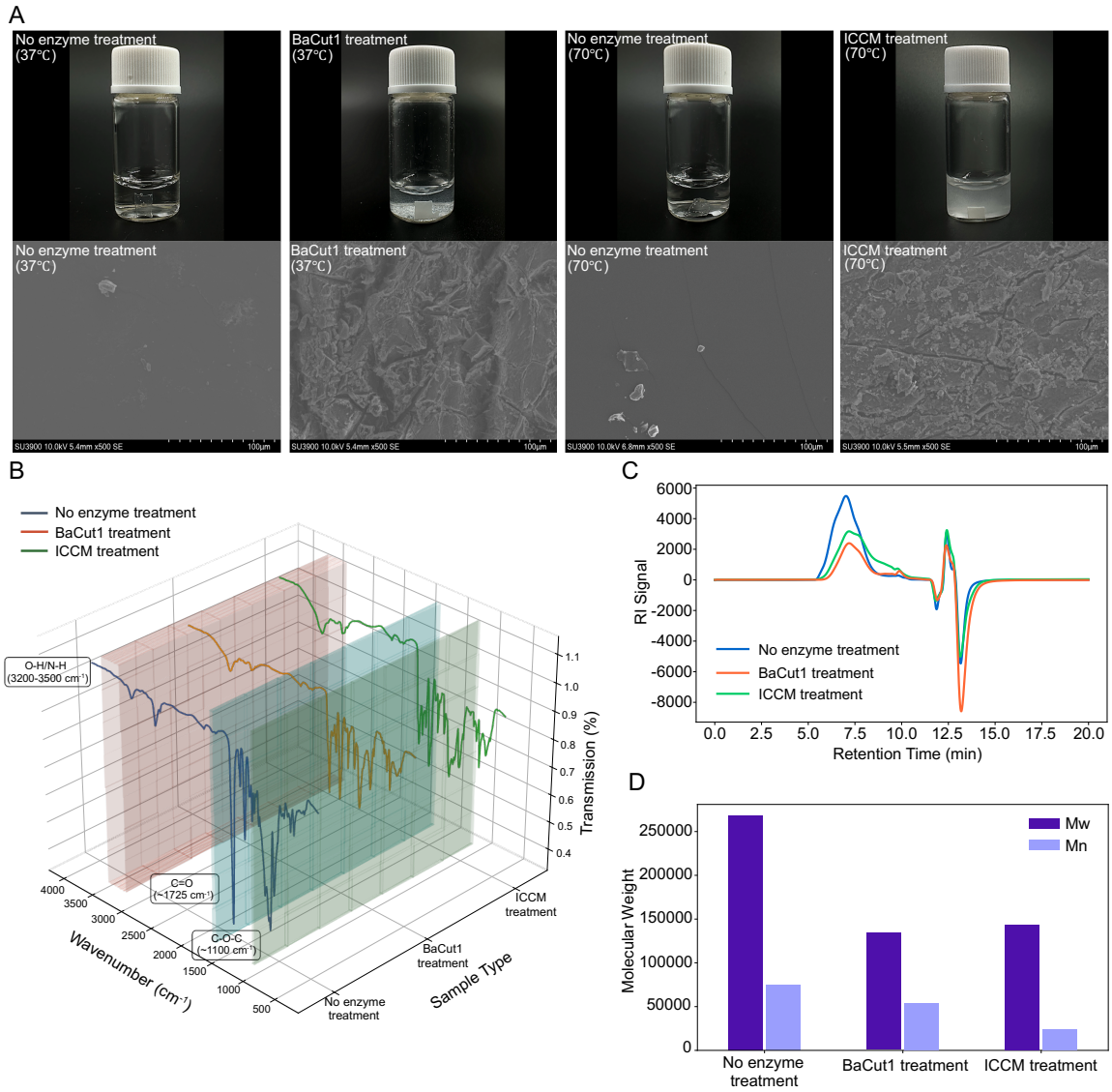

Figure 2: Enzymatic degradation of poly (ethylene adipate)-polyurethane (PEA-PU). (A) Visual observation of film degradation & Surface morphology by SEM. PEA-PU films became turbid and fragmented after 36 h of incubation with ICCM (70 °C) or BaCut1 (37 °C), while enzyme-free controls remained optically transparent, indicating enzyme-specific hydrolytic activity. **(B) FTIR spectral changes following degradation**. **(C) GPC chromatograms**. GPC analysis was performed using DMF as the mobile phase after heat-assisted dissolution. **(D) Quantification of molecular weight reduction**.

Further structural analysis by FTIR provided additional insights (Fig. 2B). Compared to untreated PEA-PU, enzyme-treated samples exhibited: (i) a broadened and slightly intensified O–H/N–H stretching band (3200–3500 cm^{-1}), consistent with an increased contribution of hydroxyl-containing chain-end functionalities arising from ester bond hydrolysis; (ii) a notable decrease in ester carbonyl (~1725 cm^{-1}) and C–O–C stretching (~1100 cm^{-1}) band intensities, confirming the breakdown of polyester segments.

To characterize the soluble degradation products, we performed chromatographic analysis of reaction supernatants. The PU monomer AA was quantified via HPLC, while EG was detected by gas chromatography. Both monomers were exclusively present in enzyme-treated samples, with no detectable levels in negative controls. Notably, the observed AA:EG molar ratio (approximately 1:1) matched the theoretical stoichiometry of PEA-PU hydrolysis, wherein each ester bond cleavage generates equimolar AA and EG (Table S1). This stoichiometric agreement establishes AA production as a robust quantitative indicator of EG release during enzymatic degradation.

Gel permeation chromatography (GPC) was then employed to quantify changes in polymer molecular weight following enzymatic treatment. Untreated PEA-PU exhibited a high molecular weight distribution, with a main retention time around 8.5 min. After enzymatic degradation, the distribution shifted toward higher retention times. Specifically, the main peak shifted to ~10.0 min after ICCM treatment and to ~9.2 min after BaCut1 treatment (Fig. 2C), consistent with the formation of lower-molecular-weight fragments. ICCM treatment led to a 67.9% reduction in number-average molecular weight (Mn) and a 47.3% reduction in weight-average molecular weight (Mw) (Fig. 2D), indicating substantial fragmentation into smaller oligomers. BaCut1 caused a relatively smaller but still significant decrease in Mn (~28.2%) and Mw (~48.5%). The corresponding polydispersity index (PDI) values are provided in Fig. S4. These molecular-level changes align with the distinct surface erosion patterns observed by SEM.

Collectively, our integrated approach—combining microscopic, spectroscopic, chromatographic, and computational analyses—demonstrates that the chemically defined PEA-PU offers exceptional analytical tractability during enzymatic degradation. Upon enzymatic treatment, PEA-PU undergoes clear morphological changes—often visible to the naked eye—and generates well-defined soluble products. These monomers can be accurately identified and quantified using conventional chromatographic methods. Importantly, by assessing PEA-PU degradation with two established PU-degrading enzymes, we confirmed that this substrate reliably recapitulates their differential activities. The degradation profiles reflect enzyme-specific catalytic behaviors, enabling robust comparative analysis of PU-hydrolyzing activity. Given these attributes, PEA-PU emerges as an ideal model substrate for comparative enzyme characterization, providing a reliable basis for quantitative PU assay development.

2.3 Development of a coupled fluorescence assay for EG detection in PEA-PU degradation

The well-defined chemical composition, transparency, and homogeneity of PEA-PU enable direct observation and quantification of enzymatic degradation, with breakdown products readily analyzed by chromatography. However, like conventional substrates, PEA-PU has a critical limitation: while chromatographic analysis offers precise quantification, its low throughput hinders large-scale enzyme screening applications. To overcome this bottleneck, we designed an enzymatic cascade that converts the stoichiometric release of EG during PU hydrolysis into a sensitive fluorescent signal (Fig. 3A).

In this coupled system, we employed an NAD^+-dependent glycerol dehydrogenase (GldA) from *Enterobacter aerogenes* [35] to oxidize EG to glyoxylic acid while reducing NAD^+ to NADH. The resulting NADH is then used by diaphorase from *Clostridium kluyveri* [36] to reduce resazurin into resorufin, a highly fluorescent dye. This two-step enzymatic cascade ensures a direct, molecule-to-molecule correspondence between PU hydrolysis (EG release) and fluorescence intensity, enabling continuous and quantitative monitoring without extensive sample processing.

To establish robust performance of the coupled enzymatic fluorescence assay, we systematically optimized its reaction conditions. We began by evaluating buffer systems to maximize GldA activity. To avoid interference from downstream enzymes, GldA was assessed independently using EG as the substrate. NADH formation was monitored at 340 nm as a direct readout of enzymatic activity. We tested six biological buffers: 50 mM Tris-HCl (pH 8.0 and 7.4), PBS (pH 8.0 and 7.4), HEPES (pH 7.4), and KH_2PO_4 (pH 8.0). Among these, KH_2PO_4 (pH 8.0) generated the highest NADH signal but exhibited poor reproducibility with significant inter-experimental variability. In contrast, 50 mM Tris-HCl (pH 8.0) supported consistently strong and stable NADH production with minimal variability (Fig. 3B). Additionally, Tris-HCl (pH 8.0) has been commonly used in prior studies involving diaphorase, supporting its suitability for the downstream coupling reaction. Based on these results, we selected 50 mM Tris-HCl (pH 8.0) as the standard buffer for all subsequent experiments.

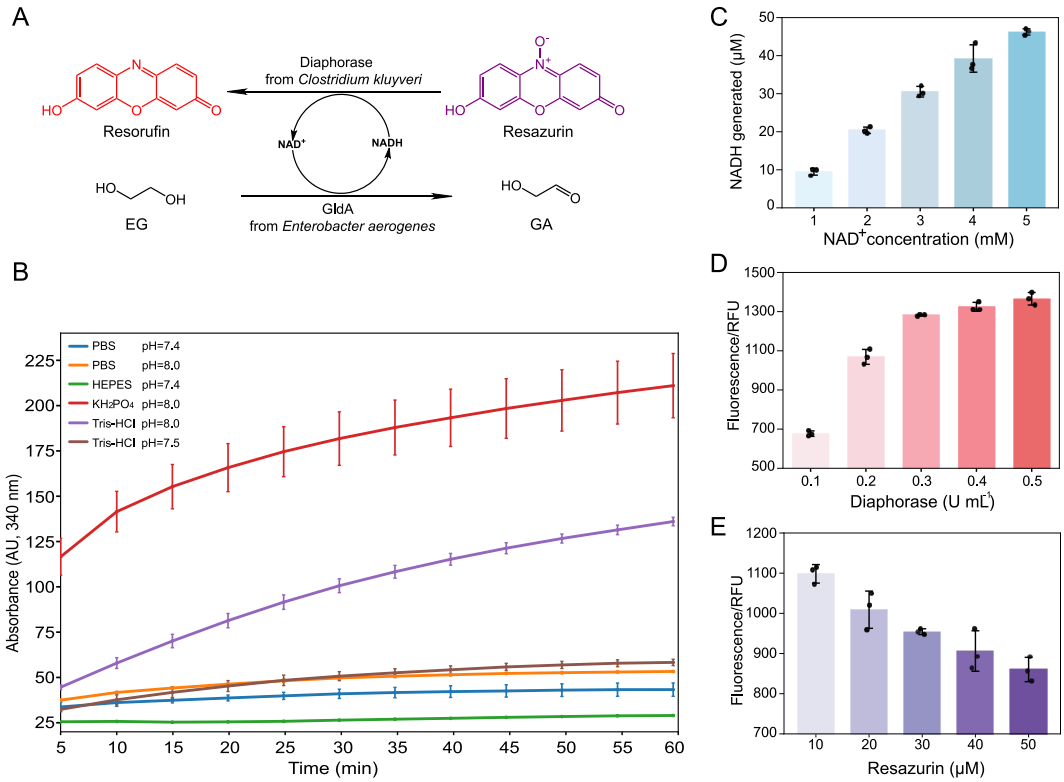

Figure 3: Development of the coupled fluorescence assay. (A) Reaction scheme of the ethylene glycol (EG)-coupled fluorescence assay. Schematic of the enzymatic cascade linking EG oxidation to resorufin fluorescence via GldA and diaphorase. **(B) Identification of the optimal buffer for GldA-mediated NADH generation. (C) Optimization of NAD^+ concentration for maximal EG oxidation. (D) Optimization of diaphorase dosage for efficient signal conversion. (E) Selection of optimal resazurin concentration to avoid quenching.**

Next, we determined the optimal concentration of the NAD^+ cofactor. Increasing NAD^+ from 1 mM to 3 mM accelerated NADH production, monitored via 340 nm absorbance (Fig. 3C). As NADH was produced in micromolar quantities, 3 mM NAD^+ was sufficient to drive the reaction and yield a stable signal; further increases in NAD^+ provided minimal additional benefit. Therefore, 3 mM was selected as the optimal concentration for subsequent assays (Fig. 3C).

We next optimized the concentration of diaphorase to ensure efficient signal transduction. Diaphorase activity was assessed by measuring fluorescence output using 20 μM NADH and 10 μM resazurin in 50 mM Tris-HCl (pH 8.0). Enzyme concentrations ranging from 0.1 U/mL to 0.5 U/mL were tested. After 30 minutes of incubation at room temperature, fluorescence (Ex/Em = 535/588 nm) increased with diaphorase concentration, plateauing at 0.3 U/mL. This suggests that 0.3 U/mL is sufficient for near-maximal signal output, with higher concentrations offering only marginal gains. Thus, 0.3 U/mL was selected as the optimal diaphorase concentration (Fig. 3D).

Finally, we evaluated resazurin, the fluorescent reporter, using 0.3 U/mL diaphorase and 20 μM NADH while varying resazurin (10–50 μM). Following the same incubation and detection protocol, fluorescence intensity decreased progressively with increasing resazurin concentrations. The highest signal was observed at 10 μM, suggesting that excess resazurin may induce self-quenching or inner-filter effects. Based on these results, 10 μM was selected as the standard resazurin concentration (Fig. 3E).

Through systematic optimization, we established a highly sensitive and reliable fluorescence-based assay for quantifying EG production from PU degradation. Under the finalized conditions (50 mM Tris-HCl, pH 8.0; 3 mM NAD^+; 10 μM resazurin; 0.3 U/mL diaphorase), the assay delivers a strong, EG-dependent fluorescent signal across a broad detection range (0.25–25 mM EG), effectively capturing expected concentrations from polymer breakdown. The fluorescence generation rate (Relative Fluorescence Units, RFU) showed excellent linear correlation with EG concentration ($R^2 > 0.99$ at all-time points from 30–120 minutes, measured at 10-minute intervals; Table S2), demonstrating both precision and temporal stability. This assay enables continuous, high-throughput monitoring of PU degradation, making it well-suited for enzyme activity screening.

2.4 Validation of the coupled fluorescence assay for PEA-PU degradation

To evaluate the quantitative performance of our coupled fluorescence assay, we first constructed calibration curves using EG standards ranging from 0.25 mM to 25 mM. Fluorescence generation rates (RFU/min), measured between 30 minutes and 120 minutes, exhibited a highly linear response (R^2 = 0.9995; Figure 4A). The limit of detection (LOD) and limit of quantification (LOQ) for EG were 0.36 mM and 1.10 mM, respectively (Supplementary Table S3). We then applied this calibration to quantify EG released from PEA-PU films following enzymatic degradation by ICCM and BaCut1.

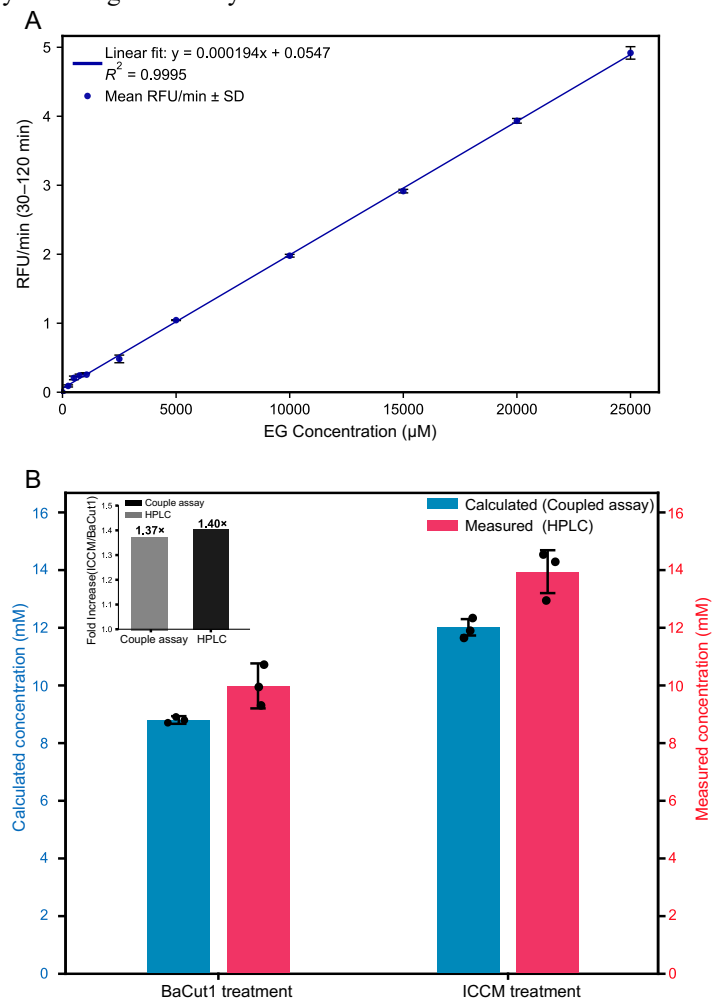

Figure 4: Validation of the coupled fluorescence assay for quantitative ethylene glycol (EG) detection. (A) Standard curve for EG detection. Fluorescence rates (RFU/min) showed excellent linear correlation with EG concentration from 0.25 to 25 mM (R^2 = 0.9995). **(B) Quantification of EG in enzymatic degradation samples.** Comparison of predicted EG concentrations (blue; derived from the fluorescence assay) and measured AA concentrations (magenta; determined by HPLC) in supernatants from PEA-PU films treated with BaCut1 and ICCM. Values reflect mean ± SD from three independent enzymatic reactions.

Inset, Fold difference in enzymatic activity between ICCM and BaCut1 as determined by the fluorescence assay (1.37×) and HPLC (1.40×), demonstrating the assay's ability to resolve enzyme-specific activity differences.

To independently validate these measurements, we used HPLC to quantify AA levels in the same samples, leveraging the known 1:1 stoichiometric co-release of EG and AA during PEA-PU hydrolysis (Table S1). Because of this relationship, HPLC-measured AA levels serve as both a robust proxy for EG production (and thus overall polymer degradation) and a direct benchmark for assessing the accuracy of fluorescence-based EG detection. Notably, fluorescence-derived EG concentrations closely matched HPLC-measured AA values (Figure 4B), confirming the assay's reliability for monitoring enzymatic degradation.

In addition to accuracy, our fluorescence assay also effectively resolved differences in enzymatic activity. As shown in Figure 4B (inset), the fluorescence assay detected a 1.37-fold greater EG release by ICCM compared to BaCut1. This ratio was highly consistent with the 1.40-fold difference measured via HPLC. This concordance underscores our fluorescence assay's capacity to discriminate subtle variations in enzyme activity, a critical feature for HTS applications.

Finally, the fluorescence assay offers several practical advantages over HPLC, including reduced analysis time, lower sample volume requirements, and inherent compatibility with microplate-based high-throughput formats. These improvements address major limitations of conventional PU degradation assays and may accelerate the discovery and engineering of enhanced PU-degrading enzymes.

2.5 HTS of BaCut1 variants using the coupled fluorescence assay

Having validated the coupled fluorescence assay as a quantitative readout of PEA-PU depolymerization, we next assessed its applicability as a HTS platform for identifying efficient PU-degrading enzymes. To this end, we applied the assay to screen a rationally designed library of BaCut1 variants in a HTS setting. In this proof-of-concept study, we successfully screened 1,344 variants within approximately 15 hours, establishing a scalable, robust workflow suitable for processing large enzyme libraries (Fig. 5A; Fig. S6).

To overcome the bottleneck of protein purification in HTS, we implemented the cSAT (self-assembling tag) system [37], which facilitated the rapid isolation of tag-free enzymes from small-volume cultures. Benchmarking confirmed that cSAT 2.0-processed BaCut1 exhibited depolymerization kinetics comparable to conventionally purified His-tagged enzyme (Fig. 5B), ensuring that the high-throughput production method preserves enzymatic function.

The library was constructed by saturating 11 substrate-proximal residues of BaCut1. Following transformation into *Escherichia coli* (*E. coli*), 1,344 colonies were arrayed by colony picking into 96-deep-well plates for expression. These variants were screened against solid PEA-PU powder, with EG release quantified via the coupled fluorescence assay (Fig. 5A). To ensure rigorous selection, we employed a composite ranking strategy, selecting the top 10 variants (0.7% of the library) for sequencing and follow-up characterization (Table S4). These variants (excluding one that failed purification) were subjected to time-resolved depolymerization assays on PEA-PU powder, with product release quantified by HPLC (Fig. 5C).

As shown in Fig. 5C, the screening successfully identified four standout variants (T30V, T30F, F165W and F165V) that exhibited activity superior to WT BaCut1. Specifically, they exhibited catalytic improvements ranging from 13.8% to 63.2% over WT BaCut1. Crucially, our workflow successfully detected depolymerization activity for E24A, a variant previously reported to be inactive by conventional assays relying on soluble surrogate substrates. By screening directly on the authentic PEA-PU substrate, our assay

circumvented the "surrogate substrate bias" that often leads to false negatives in conventional esterase screens, thereby providing a more accurate assessment of PU-degrading potential.

To verify that these activity gains translate to industrially relevant materials, the top four variants were challenged with commercial PU foam. All selected variants induced progressive disintegration of the foam over 12 hours, yielding fragmented residues (Fig. 5D). This confirms that the structure-activity relationships established using the synthetic PEA-PU substrate are predictive of performance on complex, commercial PU waste.

Structural modeling provides mechanistic insight into these activity enhancements. The beneficial mutations cluster at positions T30 and F165, which flank the entrance to the active-site pocket (Fig. 5E). In WT BaCut1, T30 contributes a polar hydroxyl group at this interface; substitution with hydrophobic residues (Val, Phe) likely alters the local solvation environment, favoring the engagement of the hydrophobic polymer chain. Furthermore, the introduction of a bulky aromatic side chain in T30F and F165W, or the reduction of steric bulk in F165V, suggests that remodeling the steric contour of the active-site entrance is critical for accommodating the bulky polymer backbone. These results identify the active-site entrance as a key "evolvable hotspot" for optimizing BaCut1 toward PU substrates.

Collectively, these findings establish a robust and scalable pipeline for the discovery and engineering of PU-degrading enzymes. By integrating a rapid fluorescence-based primary screen of 1,344 variants with product-linked HPLC validation, we demonstrate a reliable strategy for identifying sustained activity gains while circumventing the limitations of soluble surrogate assays. The successful isolation of four variants with enhanced catalytic efficiency directly validates the sensitivity and accuracy of this HTS platform. Furthermore, the confirmed efficacy of these hits on commercial PU foam underscores the platform's practical utility for engineering biocatalysts suited for complex plastic waste (Fig. 5D). Beyond BaCut1, this modular pipeline is readily adaptable to other polyester-PU hydrolases and can be scaled via automated liquid handling, offering a generalizable framework for accelerating the evolution of PU-degrading enzymes.

289

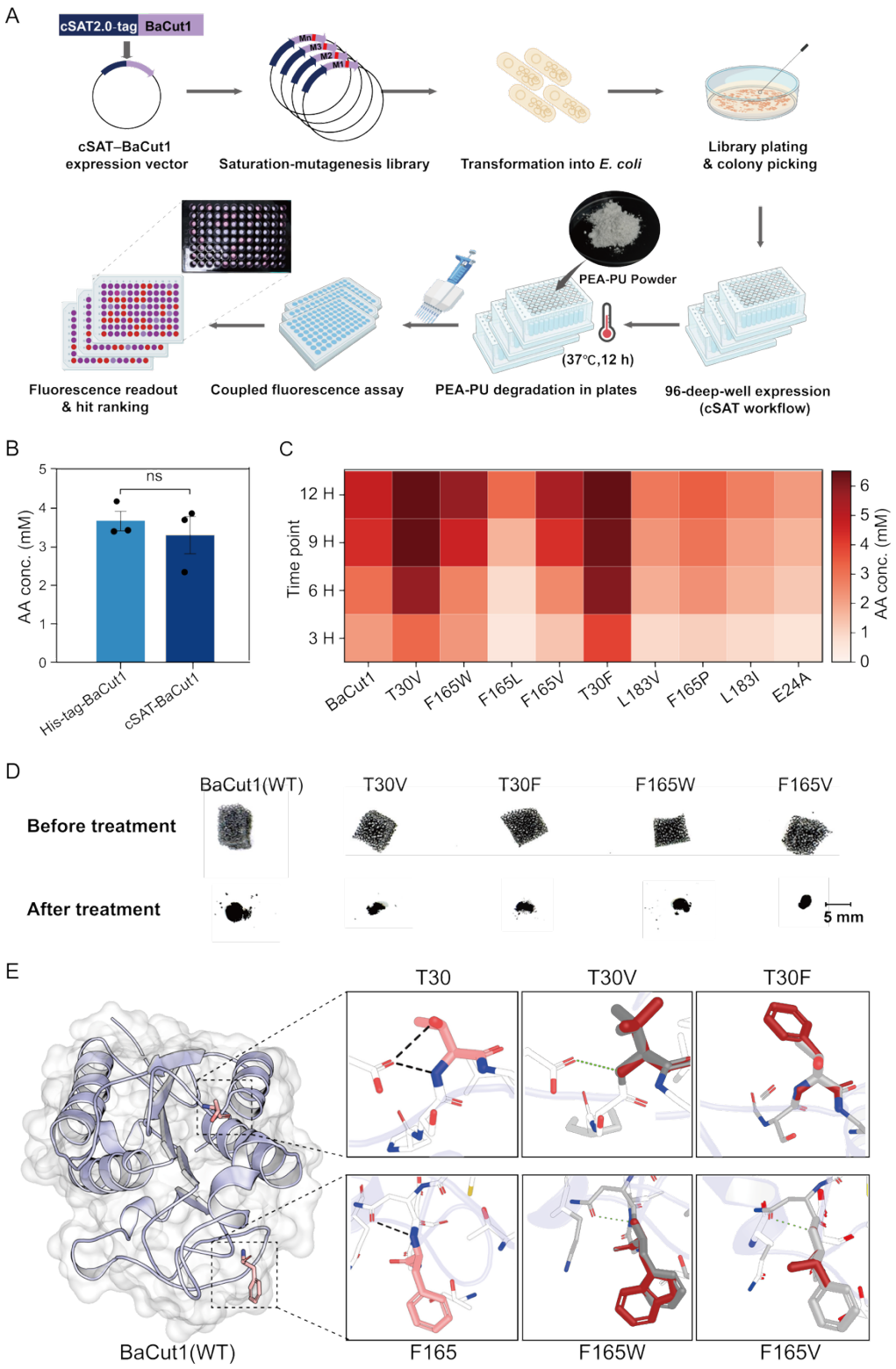
A
cSAT2.0-tag
BaCut1
cSAT–BaCut1 expression vector
Saturation-mutagenesis library
Transformation into E. coli
Library plating & colony picking
PEA-PU Powder
(37℃,12 h)
Fluorescence readout & hit ranking
Coupled fluorescence assay
PEA-PU degradation in plates
96-deep-well expression (cSAT workflow)
B
ns
AA conc. (mM)
His-tag-BaCut1
cSAT-BaCut1
C
Time point
12 H
9 H
6 H
3 H
BaCut1
T30V
F165W
F165L
F165V
T30F
L183V
F165P
L183I
E24A
AA conc. (mM)
D
BaCut1(WT)
T30V
T30F
F165W
F165V
Before treatment
After treatment
5 mm
E
T30
T30V
T30F
BaCut1(WT)
F165
F165W
F165V

Figure 5: High-throughput screening (HTS) and characterization of improved BaCut1 variants for PU degradation. (A) Schematic representation of the integrated HTS workflow. The pipeline encompasses saturation mutagenesis, cSAT 2.0-mediated protein expression in 96-deep-well plates, and a primary screen against solid PEA-PU powder using the coupled fluorescence assay. **(B) Benchmarking of enzyme preparations.** cSAT 2.0-processed BaCut1 and purified His-tagged BaCut1 showed comparable PEA-PU depolymerization (mean ± s.d., n=3; ns by t-test). **(C) Heatmap of variant activities.** Time-resolved adipic acid (AA) release from PEA-PU powder by WT BaCut1 and the top 10 ranked variants, quantified by HPLC. **(D) Validation on commercial PU foam.** Representative images before and after 12 h incubation with WT BaCut1 or the four confirmed hits (scale bar, 5 mm). **(E) Structural interpretation of confirmed hits.** Left: Structural model of BaCut1 (WT) highlighting hotspots T30 and F165 around the active-site pocket. Right: Close-up views of the mutational sites. Black dashed lines indicate hydrogen bonds observed in the WT enzyme, whereas green dashed lines denote hydrogen bonds retained in the corresponding variants; several substitutions reduce or abolish these interactions. Substitutions at these positions likely tune the local hydrophobicity and steric contour at the pocket rim, facilitating accommodation of the bulky PEA-PU polymer chain.

3 Conclusion

The development of effective HTS assays for PU-degrading enzymes is essential for discovering and optimizing biocatalysts to combat PU pollution. Here, we present an HTS assay that integrates a chemically defined PEA-PU substrate with an enzymatic cascade, converting stoichiometrically released EG into a sensitive fluorescent signal. Our assay shows excellent correlation with conventional analytical techniques (e.g., HPLC), demonstrating comparable reliability while offering the significant advantages of high-throughput compatibility, overcoming the limitations of traditional labor-intensive methods.

A key innovation of this work lies in our substrate design. Unlike proprietary substrates such as Impranil DLN (with undefined composition and obscure degradation pathways), our PEA-PU system establishes clear structure-activity relationships, directly linking specific polymer bonds to their degradation products (AA and EG). This mechanistic clarity not only enables deeper investigation of enzymatic mechanisms but also ensures that measurements are interpretable and comparable across diverse enzymes and variants, laying a solid foundation for rational engineering.

Armed with this structurally authentic screening tool, we were able to effectively characterize a BaCut1 saturation-mutagenesis library. This campaign successfully identified variants with enhanced hydrolytic activity against both the synthetic PEA-PU and commercial PU foams. Crucially, the assay detected activity in variants previously deemed inactive by conventional surrogate assays, highlighting its ability to eliminate the "surrogate substrate bias" that often leads to false negatives. By screening directly on a solid, structurally authentic polymer, our approach ensures that identified hits possess genuine depolymerization capabilities relevant to real-world materials.

Beyond its fundamental advantages, the assay offers practical benefits, including rapid processing, minimal sample requirements, and seamless compatibility with multi-well plate formats. As evidenced by the efficicent screening of over 1,300 variants, these features significantly reduce time and resource demands, making the method particularly valuable for large-scale applications, from functional metagenomic discovery to directed evolution campaigns.

Future refinements could further enhance the assay’s versatility. Examples include extending sensitivity to additional PU bond-cleavage chemistries, such as ether- and urethane-bond scission, and implementing alternative fluorophores, enzymatic cascades, or detection modalities. The platform can also be combined with

artificial intelligence-assisted enzyme design and automated liquid handling to increase screening scale and success rates.

Ultimately, our HTS assay for PEA-PU degradation provides a robust, scalable, and mechanistically precise tool for accelerating the discovery and engineering of PU-degrading enzymes. By utilizing a structurally realistic substrate, the assay ensures that identified hits exhibit industrially relevant depolymerization activity, effectively bridging the gap between laboratory discovery and real-world PU waste degradation. This approach holds significant promise for advancing sustainable PU waste management, a critical step toward achieving a circular plastics economy.

Acknowledgements
We acknowledge the support from the Biosciences Central Research Facility (BioCRF (GZ)) and the Materials Characterization and Preparation Facility (MCPF (GZ)), both of which are central research facilities of the Hong Kong University of Science and Technology (Guangzhou) (HKUST(GZ)). Their assistance in experimental procedures and material characterization was essential to this study.

Funding sources
This work is supported by the National Natural Science Foundation of China (No. 32471547), the Guangdong Basic and Applied Basic Research Foundation (No. 2025A1515010527), the Nansha Key Science and Technology Project (No. 2023ZD015), the Guangzhou Science and Technology Program City-University Joint Funding Project (No. 2023A03J0001), and the Guangdong Science and Technology Department (No. 2025A0505000039), the Fujian Science and Technology Program Project (No. 2025I0045).

4 References

[1] R.C. Thompson, Y. Olsen, R.P. Mitchell *et al.*, Twenty years of microplastic pollution research—what have we learned, *Science* 386 (2024) eadl2746.

[2] J. Liang, Y. Yang, Q. Zhou *et al.*, Unraveling the threat: microplastics and nanoplastics' impact on reproductive viability across ecosystems, *Sci. Total Environ.* 913 (2024) 169525.

[3] V. Nava, A. Berton, A. Boggero *et al.*, Plastic debris in lakes and reservoirs, *Nature* 619 (2023) 317–322.

[4] J. Lei, Q. Li, X. Zheng *et al.*, Microplastic environmental behavior and health risk assessment: a review, *Environ. Chem. Lett.* 22 (2024) 1–29.

[5] Z. Liu, Y. Luo, Y. Liang *et al.*, Anionic nanoplastic contaminants promote Parkinson's-disease–associated α-synuclein aggregation, *Sci. Adv.* 9 (2023) eadi8716.

[6] H. Zha, M. Liu, X. Wu *et al.*, Foodborne and airborne polyethersulfone nanoplastics respectively induce liver and lung injury in mice: comparison with microplastics, *Environ. Int.* 183 (2024) 108350.

[7] H. Huang, X. Zhang, W. Li *et al.*, Microplastics in the bloodstream can induce cerebral thrombosis by causing cell obstruction and lead to neurobehavioral abnormalities, *Sci. Adv.* 11 (2025) eadr8243.

[8] B. Zhao, H. Wang, J. Liu *et al.*, The potential toxicity of microplastics on human health, *Sci. Total Environ.* 912 (2024) 168946.

[9] J. Drzeżdżon, J. Datta, Advances in the degradation and recycling of polyurethanes: biodegradation strategies, MALDI applications, and environmental implications, *Waste Manag.* 198 (2025) 21–45.

[10] Z. Li, C. Zhang, J. Chen *et al.*, Structure-guided engineering of a versatile urethanase improves its polyurethane depolymerization activity, *Adv. Sci.* 12 (2025) 2416019.

[11] D. Simón, P. Hidalgo, F. Pérez *et al.*, Recycling of polyurethanes from laboratory to industry: a journey towards the sustainability, *Waste Manag.* 76 (2018) 147–171.

[12] G. Rossignolo, G. Malucelli, A. Lorenzetti, Recycling of polyurethanes: where we are and where we are going, *Green Chem.* 26 (2024) 1132–1152.

[13] N. Gama, A. Ferreira, A. Barros-Timmons, Polyurethane recycling through acidolysis: current status and prospects for the future, *J. Polym. Environ.* 32 (2024) 4777–4793.

[14] J. Liu, Y. Li, Y. Zhang *et al.*, Biodegradation and up-cycling of polyurethanes: progress, challenges, and prospects, *Biotechnol. Adv.* 48 (2021) 107730.

[15] A. Raczyńska, A. Góra, I. André, An overview on polyurethane-degrading enzymes, *Biotechnol. Adv.* 68 (2024) 108439.

[16] R. Geyer, J.R. Jambeck, K.L. Law, Production, use, and fate of all plastics ever made, Sci. Adv. 3(7) (2017) e1700782.

[17] S.P. Katnic, F.M. de Souza, R.K. Gupta, Recent progress in enzymatic degradation and recycling of polyurethanes, Biochem. Eng. J. 204 (2024) 109363.

[18] Jiang, Yuting, et al. "PufH: A promising biocatalyst for the recycling and bioremediation of polyurethane foam waste." *Journal of Hazardous Materials* (2025): 140108.

[19] A. Magnin, E. Pollet, L. Avérous, Characterization of the enzymatic degradation of polyurethanes, *Methods Enzymol.* 648 (2021) 317–336.

[20] H. Puetz, D. Yamamoto, L.M. Blank *et al.*, Validated high-throughput screening system for nylon-depolymerizing enzymes, *ACS Sustain. Chem. Eng.* 11 (2023) 15513–15522.

[21] C. Acevedo-Rocha, M. Pérez-Gallego, F.H. Arnold *et al.*, Artificial, biomimetic and hybrid enzymes: general discussion, *Faraday Discuss.* 252 (2024) 354–386.

[22] A. Magnin, E. Pollet, L. Avérous, Evaluation of biological degradation of polyurethanes, *Biotechnol. Adv.* 39 (2020) 107457.

[23] M. Cregut, M. Bedas, M.J. Durand, G. Thouand, New insights into polyurethane biodegradation and realistic prospects for the development of a sustainable waste recycling process, *Biotechnol. Adv.* 31 (2013) 1634–1647.

[24] M.-T. Kuo, J.F. Raffaelle, E.M. Waller, V.A. Varaljay, D. Wagner, N. Kelley-Loughnane, N.F. Reuel, Screening Enzymatic Degradation of Polyester Polyurethane with Fluorescent Single-walled Carbon Nanotube and Polymer Nanoparticle Conjugates, ACS Nano 17(17) (2023) 17021–17030.

[25] A. Xu, J. Liu, S. Cao *et al.*, Application of a novel fluorogenic polyurethane analogue probe in polyester-degrading microorganisms screening by microfluidic droplet, **Microb. Biotechnol.** 16(2) (2023) 474–480.

[26] J.C. Biffinger, J.T. Wertz, D.T. Fox *et al.*, The applicability of Impranil DLN for gauging the biodegradation of polyurethanes, *Polym. Degrad. Stab.* 120 (2015) 178–185.

[27] J. Liu, X. Wang, Y. Li, Y. Jiang, Y. Zhang, Biodegradation of polyester polyurethane by *Cladosporium* sp. P7: evaluating its degradation capacity and metabolic pathways, *J. Hazard. Mater.* 448 (2023) 130776.

[28] A. Magnin, E. Pollet, L. Avérous, Isolation and characterization of different promising fungi for biological waste management of polyurethanes, *Microb. Biotechnol.* 12 (2019) 544–555.

[29] W. Sikorska, G. Janowska, W. Musial *et al.*, Synthesis and physicochemical properties of new (bio)degradable poly(ester-urethane)s containing polylactide and poly[(1,4-butylene terephthalate)-co-(1,4-butylene adipate)] segments, *Polymer* 52 (2011) 4676–4685.

[30] P. Pfohl, D. Bahl, M. Rückel et al., Effect of polymer properties on the biodegradation of polyurethane microplastics, *Environ. Sci. Technol*. 56(23) (2022) 16873–16884.

[31] V. Tournier, C.M. Topham, A. Gilles et al., An engineered PET depolymerase to break down and recycle plastic bottles, *Nature* 580(7802) (2020) 216–219.

[32] H. Lu, D.J. Diaz, N.J. Czarnecki *et al.*, Machine learning–aided engineering of hydrolases for PET depolymerization, *Nature* 604 (2022) 662–667.

[33] Z. Jiang, Z. Li, L. Wang, H. Lu, Novel polyurethane-degrading cutinase BaCut1 from *Blastobotrys* sp. G-9 with potential role in plastic bio-recycling, *J. Hazard. Mater.* 472 (2024) 134493.

[34] Eberhardt, Jerome, et al. "AutoDock Vina 1.2. 0: new docking methods, expanded force field, and python bindings." Journal of chemical information and modeling 61.8 (2021): 3891-3898.

[35] A.B. Filip, J.E. Hardy, T.H. Jones *et al.*, Accuracy of a glycerol dehydrogenase assay for ethylene glycol detection, *J. Med. Toxicol.* 19 (2023) 362–367.

[36] M. Gimeno-Pérez, X. Chen, R. Mezzenga, A coupled ketoreductase–diaphorase assay for the detection of polyethylene terephthalate–hydrolyzing activity, *ChemSusChem* 15 (2022) e202102750.

[37] Huang, Yuan, et al. "A high-performance protein preparation approach in a single column-free step." Trends in Biotechnology 43.2 (2025): 476-487.

5 Materials and Methods

5.1 Materials

Unless otherwise stated, all reagents were of analytical grade and used as supplied. Hydroxyl-terminated poly(ethylene adipate) (PEA, Mn ≈ 1000 g/mol, CAS No. 24938-37-2), 4,4′-methylenebis (phenyl isocyanate) (MDI, CAS No. 101-68-8), and anhydrous N, N-dimethylformamide (DMF, CAS No. 68-12-2) were purchased from Aladdin Industrial Corporation (Shanghai, China).

Resazurin (≥98%, CAS No. 550-82-3) and Diaphorase from *Clostridium kluyveri* (3.0-20.0 units/mg protein, CAS No. 9001-18-7) were purchased from Sigma-Aldrich (St. Louis, MO, USA). β-Nicotinamide adenine dinucleotide (NAD^+, >98%, CAS No. 53-84-9) was obtained from Roche Diagnostics GmbH (Mannheim, Germany).

The polyurethane-degrading enzymes ICCM and BaCut1 were prepared as described previously. BaCut1, based on the reported sequence from *Blastobotrys* sp. G-9 (DOI:10.1016/j.jhazmat.2024.134493), was codon-optimized, synthesized (Tsingke Biotechnology Co., Ltd., Beijing, China), and cloned into the pET28a expression vector. ICCM (an engineered LCC variant; F243I/D238C/S283C/N246M; DOI:10.1038/s41586-022-04599-z) and glycerol dehydrogenase (GldA) from *Enterobacter aerogenes* were obtained from in-house laboratory stocks; GldA expression and purification followed the procedure described in Section 5.2.4.

All other routine chemicals, buffer components (e.g., Tris base, NaCl, imidazole), and consumables were purchased from Sigma-Aldrich unless otherwise stated. Ultrapure water (18.2 MΩ·cm) was prepared using a Milli-Q® Integral water purification system (Merck Millipore, USA). Black, flat-bottom, low-volume 96-well plates were obtained from Corning® (Corning, NY, USA) for fluorescence measurements.

5.2 Methods

5.2.1. Synthesis of PEA-PU Films

PEA was vacuum-dried at 120 °C for 1 h prior to use. In a nitrogen-purged three-neck flask, PEA and MDI were dissolved in anhydrous DMF (10% w/v) at an NCO:OH equivalent ratio of 1:1. The reaction mixture was stirred at 70 °C for 1 h under a dry nitrogen atmosphere. The resulting viscous prepolymer was cast into a PTFE mold and vacuum-dried at 60 °C for 24 h, yielding uniform transparent films of approximately 0.2 mm thickness. Films were stored in a desiccator prior to use.

5.2.2. Preparation of freeze-milled PEA-PU powder

To enable rapid and reproducible enzyme–substrate contact in microplate formats, PEA-PU films were converted to a powder substrate by cryogenic processing. Briefly, PEA-PU films were cut into small pieces and pre-frozen in liquid nitrogen for 3 h, then immediately subjected to cryogenic grinding using a grinding mill under cold conditions to prevent thermal softening and particle fusion. The resulting powder was kept dry, warmed to room temperature in a closed container to minimize moisture condensation, and stored in a desiccator until use.

5.2.3. Structural and Thermal Characterization

^{1}H NMR spectra were recorded on a Bruker Avance III 400 MHz spectrometer using DMSO-d_6 as solvent. Chemical shifts were referenced to the residual solvent peak at δ 2.50 ppm.

ATR-FTIR spectra were obtained using a Bruker Vertex 70V FTIR spectrometer coupled with a Hyperion II microscope (Bruker, Germany), operated at 4 cm^{-1} resolution with 32 scans per sample.

Differential scanning calorimetry (DSC) measurements were performed on a DSC 2500 (TA Instruments, New Castle, DE, USA). Approximately 5 mg of each PEA-PU film was sealed in an aluminium Tzero™ pan with a matching lid. Samples were equilibrated at –50 °C for 1 min, heated to 200 °C at 10 °C min^{-1}, held for 1 min, cooled to –50 °C at the same rate, and then reheated to 200 °C. Thermograms from the second heating scan were used for analysis to remove thermal-history effects. The glass-transition temperature was determined from the midpoint of the heat-capacity step in the second heating trace.

SEM analysis was conducted to assess surface morphology before and after enzymatic degradation. Samples were sputter-coated with a thin layer of platinum to ensure conductivity. Imaging was performed using a Hitachi SU3900 Scanning Electron Microscope at an accelerating voltage of 10.0 kV, a working distance of 5.4 mm, and a magnification of ×500 under secondary electron (SE) mode. Scale bars were set to 100 µm.

5.2.4. Protein Expression and Purification

5.2.4.1. Conventional His6-tag expression and Ni-affinity purification

The enzymes GldA, ICCM, and BaCut1 were recombinantly expressed and purified for this study. The corresponding genes for each enzyme were cloned into the pET28a(+) expression vector, which incorporates a C-terminal His_6-tag for affinity purification. The resulting plasmids were transformed into *E. coli* BL21(DE3) host cells.

For protein expression, cultures were grown in Luria-Bertani (LB) medium containing 50 µg/mL Kanamycin at 37 °C with vigorous shaking until the optical density at OD_{600} reached 0.6–0.8. Protein synthesis was then induced with a final concentration of 0.2 mM isopropyl β-D-1-thiogalactopyranoside (IPTG), and the cultures were further incubated at 16 °C for 16–20 h.

After incubation, cells were harvested by centrifugation (4,000 × g, 30 min, 4 °C), and the cell pellet was resuspended in lysis buffer (50 mM Tris-HCl, pH 8.0, 150 mM NaCl). The cells were disrupted by sonication on ice, and the crude lysate was clarified by high-speed centrifugation (30,000 × g, 30 min, 4 °C) to remove cell debris.

The clarified supernatant was loaded onto a Ni Sepharose 6 Fast Flow affinity column (Cytiva) pre-equilibrated with the lysis buffer. The column was washed with the same buffer containing 20 mM imidazole to remove non-specifically bound proteins. The target His-tagged protein was subsequently eluted using a buffer containing 300 mM imidazole. The eluted fractions were desalted and concentrated using Amicon® Ultra-15 centrifugal filters (10 kDa MWCO, Merck Millipore). The purity of the final protein samples was confirmed by SDS-PAGE, and their concentrations were determined spectrophotometrically at 280 nm using a NanoDrop™ 2000 spectrophotometer (Thermo Fisher Scientific).

5.2.4.2. cSAT2.0-based preparation of tag-free enzymes for high-throughput screening

To enable rapid preparation of enzymes for high-throughput screening, target proteins were expressed as N-terminal cSAT2.0-tag fusions, in which the cSAT2.0 tag is linked to the target enzyme through a pH-responsive intein.

For 96-deep-well HTS-scale preparation, *E. coli* BL21(DE3) cultures were grown in 1 mL LB per well under the same induction conditions (Section 5.2.4.1.). Cells were harvested by centrifugation (4000 × g, 20 min, 4 °C). Pellets were lysed using BeyoLytic Bacterial Active Protein Extraction Reagent (Beyotime, P0013Q), which enables one-step extraction; lysis was performed for 15 min according to the manufacturer's instructions. The lysates were centrifuged (4000 × g, 20 min, 4 °C) to compact insoluble material. The supernatant was removed, and the pellet was washed twice with Buffer B1 (20 mM Tris-HCl, 500 mM NaCl, 1 mM EDTA, pH 8.5). The washed pellet was then resuspended in 150 µL of Buffer B2 (40 mM Bis–Tris, 2 mM EDTA, 300 mM NaCl, pH 6.2) and incubated at 25 °C for 24 h to trigger intein-mediated cleavage and release of the target enzyme.

5.2.4.3. Protein expression in shake flasks for cSAT processing (BaCut1 and variants)

To obtain enough purified enzymes for biochemical characterization, BaCut1 and its variants were expressed as N-terminal cSAT2.0-tag fusions. Large-scale cultivation was performed in shake flasks containing 400 mL of LB medium supplemented with 50 µg/mL kanamycin. Recombinant *E. coli* BL21(DE3) strains were initially grown at 37 °C with shaking at 200 rpm. When the OD_{600} reached 0.6–0.8, the temperature was shifted to 18 °C, and protein expression was induced by the addition of IPTG to a final concentration of 0.2 mM. After 24 h of induction, the cells were harvested by centrifugation (4000 × g, 20 min, 4 °C). The resulting cell pellets were either processed immediately for intein-mediated purification.

5.2.5. Enzymatic Degradation of PEA-PU Films and Freeze-milled Powder

PEA-PU films were cut into 0.8 cm × 0.8 cm squares. Each film sample was incubated in 1.0 mL of 50 mM Tris-HCl buffer (pH 8.0) containing ICCM (13.95 µg/mL) or BaCut1 (125 µg/mL) at their respective optimal temperatures (70 °C and 37 °C) for 36 hours. Control samples lacked enzyme. Reaction supernatants were collected for product analysis. All film degradation reactions were performed under static incubation.

For powder-based degradation at preparative scale, freeze-milled PEA-PU powder was used as a suspended solid substrate. Reactions were performed by incubating PEA-PU powder (2 mg per reaction) in 1.0 mL of 50 mM Tris-HCl buffer (pH 8.0) supplemented with $CaCl_2$ (30 mM), with BaCut1 or BaCut1 variants (as indicated). Incubations were carried out at 37 °C for 12 h with gentle agitation to maintain polymer suspension. After incubation, reaction mixtures were clarified by centrifugation to remove residual polymer particles and further filtered through a 0.22 µm membrane.

5.2.6. Chromatographic Analysis of Degradation Products

To validate the enzymatic degradation of PEA-PU films, the resulting hydrolysis products were detected using gas chromatography and high-performance liquid chromatography.

Gas Chromatography–Flame Ionization Detection (GC-FID):

Ethylene glycol (EG) in the enzymatic degradation supernatants was analyzed by a third-party analytical laboratory using a Shimadzu GC system equipped with a flame ionization detector (FID). EG was detected at a retention time of approximately 4.73 minutes. Quantification was based on an external standard calibration curve (5–20 ppm), which showed excellent linearity ($R^2 > 0.998$).

High-Performance Liquid Chromatography (HPLC)：

Adipic acid (AA) was analyzed using a Thermo Scientific Vanquish Core HPLC system (Thermo Fisher Scientific, Germany) equipped with a Shim-pack GIST C18 AQ column (3 μm, 150 mm × 4.6 mm; Shimadzu, Japan). The mobile phase consisted of 0.1% trifluoroacetic acid (TFA) in water (solvent A) and acetonitrile (solvent B). Gradient elution was performed as follows: 0–20 min, 5–95% B; 20–24 min, held at 95% B; 24–25 min, ramped back to 5% B; followed by a 5-minute re-equilibration at 5% B. The flow rate was 1.0 mL/min, the detection wavelength was set at 210 nm, and the injection volume was 10 μL. Quantification was based on an external calibration curve (1–100 ppm), which showed excellent linearity ($R^2 > 0.999$).

5.2.7. Coupled Fluorescence Assay for EG Detection

A fluorescence-based coupled enzyme assay was developed to quantify ethylene glycol (EG) released from PEA-PU degradation. Reactions were performed in black 96-well plates with a final volume of 200 μL. Each reaction contained 50 mM Tris-HCl buffer (pH 8.0), 3 mM NAD^+, 10 μM resazurin, 0.3 U/mL diaphorase, 0.25 mg/mL GldA, and either EG standards or samples.

To construct the standard curve, EG standards (0.25–25 mM) were prepared in assay buffer and incubated at room temperature. Fluorescence was monitored at Ex/Em = 535/588 nm using a Thermo Scientific Varioskan™ LUX microplate reader in kinetic mode for 180 minutes, with readings collected every 5 minutes. The fluorescence rate (RFU/min) was plotted against EG concentration, yielding a linear regression with $R^2 \geq 0.9995$.

For experimental samples, 20 μL of degradation supernatant was added to 180 μL of assay buffer. Fluorescence was recorded under identical conditions, and EG concentrations were interpolated from the standard curve. All measurements were performed in triplicate.

5.2.8. Library Construction and High-Throughput Screening

Library construction and expression. Single-site saturation mutagenesis libraries of BaCut1 were constructed using the NNK strategy targeting 11 residues. For HTS, BaCut1 variant libraries were designed as N-terminal cSAT2.0–intein fusions and cloned into the pET28a(+) backbone. Variant expression was performed in 96-deep-well plates (1 mL LB per well) under the induction conditions described in Section 5.2.4. Enzymes were prepared as tag-free crude enzyme preparations using the cSAT2.0 workflow (Section 5.2.4.2), without chromatographic purification.

Primary screening on freeze-milled PEA-PU powder. Primary reactions were performed in 96-well format by incubating tag-free crude enzyme preparations with freeze-milled PEA-PU powder (2 mg per well) in 50 mM Tris-HCl buffer (pH 8.0) supplemented with $CaCl_2$ (30 mM). Reactions were carried out at 37 °C for 12 h with continuous agitation to maintain polymer suspension and ensure reproducible enzyme–substrate contact. After incubation, reaction mixtures were clarified to remove residual polymer particles by filtration (0.22 μm). Clarified supernatant (20 μL) was then mixed with coupled assay reagents (180 μL) containing 3 mM NAD^+,

566 10 μM resazurin, 0.3 U/mL diaphorase, and 0.25 mg/mL GldA in 50 mM Tris-HCl (pH 8.0). Fluorescence was
567 monitored at Ex/Em = 535/588 nm, and the reaction rate (RFU/min) was used as the primary quantitative
568 readout of EG release.

569 Hit calling and ranking. RFU/min values were background-corrected using enzyme-free controls. To minimize
570 plate-to-plate variability, results were normalized within each plate using internal reference wells, and
571 candidates were prioritized based on a combined ranking that considered both (i) global performance across the
572 full dataset and (ii) intra-plate ranking relative to plate controls, thereby reducing bias from local
573 growth/expression variability and edge effects.

574 Confirmation by re-expression and powder-based re-screen. To confirm primary hits and exclude false positives
575 arising from expression variability, selected candidate variants were re-inoculated and re-expressed under the
576 same 96-deep-well conditions. Tag-free crude enzyme preparations were regenerated using the cSAT2.0
577 workflow (Section 5.2.4.2) and re-tested on freeze-milled PEA-PU powder under identical reaction conditions
578 as the primary screen (2 mg powder per well, 50 mM Tris-HCl pH 8.0, 30 mM $CaCl_2$, 37 °C, 12 h). EG release
579 in the clarified supernatants was quantified by the coupled fluorescence assay as described above.

580 **5.2.9. Data processing and statistical analysis**

581 All experiments were performed with at least three independent replicates unless otherwise stated. Data are
582 reported as mean ± SD. Where applicable, statistical comparisons between groups were performed using two-
583 tailed Student's t-tests, with $p < 0.05$ considered statistically significant. For fluorescence kinetics, slopes
584 (RFU/min) were obtained by linear regression within the defined linear region after background correction.